



Multi-element signatures in solid and solution phases in a tropical mixing zone: A case study in the Cai River estuary, Vietnam

Sofia E. Koukina, PhD^{a,*}, Nikolay V. Lobus, PhD^b, Alexander V. Shatrevan^{a,c}

^a Shirshov Institute of Oceanology, Russian Academy of Sciences, Nahimovskiy Pr. 36, 117997, Moscow, Russia

^b Timiryazev Institute of Plant Physiology, Russian Academy of Sciences, Botanicheskaya St. 35, 127276, Moscow, Russia

^c Prokhorov General Physics Institute of the Russian Academy of Sciences, Vavilova St. 38, 119991, Moscow, Russia

ARTICLE INFO

Handling Editor: Martine Leermakers

Keywords:

Nha trang bay
Estuarine gradients
Enrichment factor
Multi-element signatures
Partitioning patterns

ABSTRACT

This study provides baseline concentrations of major, trace, and rare earth elements (REEs) in the solid and solution phases of the tropical Cai River estuary under influence of multiple stresses.

The application of the selected multivariate analysis tools (principal component analysis and redundancy analysis) to the enrichment factor and partitioning coefficients ($K_{SPM/Water}$ and $K_{SPM/Sed}$) calculated from the bulk element contents highlighted the strongest relationships (considered as multi-element signatures) according to the efficiency of the transfer across the estuarine gradients (considered as a selective geochemical filter). Thus, most of the major and trace elements, and REEs studied mainly settle within the mixing zone due to the association with terrigenous aluminosilicate clay minerals, whereas Co, Ni, Cu, As, and Mo are transferred seaward because of their association with the most labile fraction of the fluvial particulate load (such as clays, organic colloids, and carbonates).

The major and trace elements, and REEs investigated in this study are mainly introduced in the Cai River and its estuary via basement rock weathering under enhanced monsoonal precipitation, whereas Bi showed the most severe enrichment in the non-weathering distribution pattern. The fractionation of the fluvial element load within the estuarine geochemical filter is mainly controlled by the differential settling of fluvial mineral element-bearing phases along with estuarine colloid dynamics – a topic that must warrants further investigation.

1. Introduction

On a global scale, transitional mixing zones of two water masses with distinct physicochemical properties (such as river confluences, mining exhausts, and estuaries) act as selective geochemical filters of both suspended and dissolved loads of major and trace elements (Guinoiseau et al., 2016).

Thus, estuaries are complex biogeochemical reactors that modify the flux and composition of terrestrial materials delivered by rivers to the ocean (Sholkovitz and Szymczak, 2000). While large rivers play a key role in the organic and terrestrial-marine linkage, 40 %–70% of the global sediment input to the oceans is transported by smaller, more abundant mountainous rivers (Bianchi, 2007).

The highly dynamic nature of estuarine systems, characterised by strong chemical and physical gradients, makes the cycling of trace elements considerably more complex in estuaries than in other aquatic systems (Bianchi, 2007; Turner, 1996). The trace elements distributed in

dissolved, colloidal, particulate, and sedimentary phases influence the coastal water quality and the health of coastal ecosystem (Iglesias et al., 2020; Tomczak et al., 2019).

To assess the potential risk element distribution, fractionation, and partitioning in aquatic systems, modern research has largely implemented subsistent multivariate techniques to ordinate bulk element content in solid and solution phases (Gaonkar and Matta, 2019; Huang et al., 2020; Lounas et al., 2020; Mali et al., 2017, 2019, 2017; Stutter et al., 2009; Varol, 2011). However, the interpretation of the distribution of bulk element content may not always be indicative in high-gradient zones such as estuaries because of complex biogeochemical processes (flocculation, adsorption, desorption, precipitation, dissolution, and redox reactions). These processes largely influence abundance and partitioning of the elements between different phases (water, suspended particulate matter (SPM), and sediments) (Gaonkar and Matta, 2019; Koiter et al., 2013; Strady et al., 2017b). Therefore, developing a comprehensive approach by combining raw data

* Corresponding author.

E-mail addresses: skoukina@gmail.com (S.E. Koukina), lobus.nikolay@gmail.com (N.V. Lobus), ashatrevan@ocean.ru (A.V. Shatrevan).

transformation with subsistent multivariate analysis tools is essential for the complete evaluation of element behaviour and mobility within the estuarine geochemical filter.

In tropical river basins, warm and humid climate with intense rainfall can lead to the rapid removal of weathering products from the source area to the sea in a relatively shorter residence time compared to a more temperate climate. Thus, estuarine regions of such river systems are ideal places for exploring trace element geochemistry (Barats et al., 2020; da Conceição et al., 2020; Fernandes et al., 2019; Lima et al., 2021; Prabakaran et al., 2019; Rousseau et al., 2019; Thanh-Nho et al., 2019).

One of the notable examples of such estuarine regions is the Cai River estuary and the adjacent part of Nha Trang Bay (South China Sea). Both of these regions have been largely exposed to multiple natural (such as heavy rainfall events, river floods, upwelling, turbidities, and major typhoons) and anthropogenic (e.g. human settlement, damming, construction, agriculture, aquaculture, mariculture, tourism, and transport)

influencing factors (Cuong et al., 2019; Giuliani et al., 2019; Lobus and Komov, 2016; Romano et al., 2013). Recently, several geochemical studies have been undertaken by primarily focusing on surface bottom sediments, although very little geochemical data on SPM and no data on water mass geochemical composition are available (Baturin et al., 2014; Koukina and Lobus, 2018, 2020, 2020; Koukina et al., 2017; Lobus et al., 2011; Tomilina et al., 2016).

Therefore, this study aims to 1) fill the existing gaps in the assessment of local geochemical baselines of solid and solution phases, and 2) gain understanding of the fate of major and trace elements transported through the estuarine geochemical filter in a small tropical estuary under multiple influencing factors.

A multivariate approach was implemented to achieve these goals. It comprised two steps: 1) calculation of the enrichment factors and partition coefficients from the raw bulk data to compare the results from different elements with drastically different abundances in water, suspended, and deposited sediments; 2) application of multivariate analysis

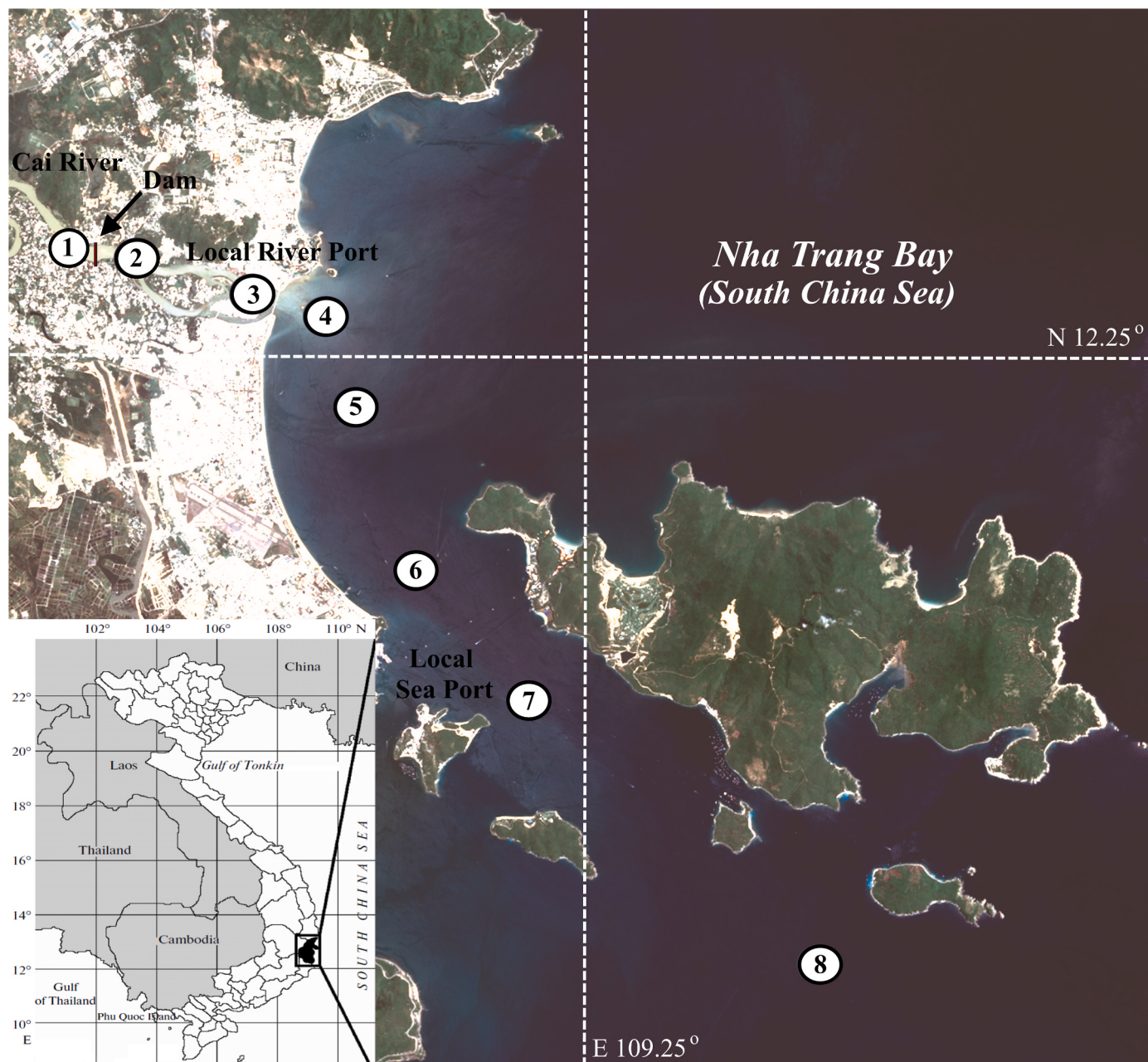


Fig. 1. Sampling site locations (Landsat 8 satellite image, 16 August 2013).

tools (principal component (PCA) and redundancy (RDA) analyses) to the enrichment factors and partition coefficient distributions to ordinate the elements according to the efficiency of their transfer across the estuarine gradients and their affinity to environmental factors (salinity, total suspended load (TSS), dissolved organic carbon (DOC), particulate organic carbon (POC), total organic carbon (TOC), total inorganic carbon (TIC), and grain size).

Therefore, this study provides new tools to evaluate element fractionation and mobility at estuarine gradients, which are considered as selective geochemical filters.

2. Materials and methods

2.1. Sampling

Surface water (eight locations, sites 1–8) and surface sediment samples (seven locations, sites 2–8) were collected in the Cai River estuary and Nha Trang Bay between July and August 2013 (Fig. 1).

Surface water samples were collected using plastic Niskin bottles. Salinity and alkalinity were measured on board using a portable conductivity apparatus HI 98129 Combo and HI 98302 DIST 2 (Hanna Instruments, Germany). The SPM samples were obtained by filtering the water samples in an all-glass filtering system. Pre-weighted polycarbonate filters (pore diameter 0.45 µm; Millipore) were used for TSS measurements, combusted glass fibre filters (GF/F, Whatman) were used for (POC, and acid-clean cellulose filters (pore diameter 0.45 µm; Millipore) were used for chemical composition analyses. After sampling, the polycarbonate and cellulose filters were rinsed with 250 ml of Milli-Q water to remove seawater salts. All the filters were dried to a constant weight at 60 °C. After filtration, the filtered water samples were placed in sterile polypropylene containers, acidified to pH 2 with 65% nitric acid (Merck) for dissolved (filtered) chemical elements (DCE), and with 35% hydrochloric acid (Merck) for DOC analyses and were kept cool until laboratory analyses.

Surface sediment samples were collected by scuba divers using a manual plastic piston corer, which was produced at the Shirshov Institute of Oceanology (Moscow, Russia). The collected samples were placed in pre-cleaned polyethylene containers using stainless-steel spatulas. One portion of the sample was kept frozen until the grain size and mineralogical analyses were performed. The other portion was dried to a constant weight at 60 °C for chemical element analysis.

All sampling, sampling transportation, and preparation procedures were performed using standard clean techniques according to the manual of Loring and Rantala (1992).

2.2. Laboratory analyses

Organic geochemistry analyses of the filtered water, SPM, and sediment samples were performed at the Ocean Chemistry Laboratory of the Shirshov Institute of Oceanology (Russian Academy of Science, RAS). The DOC, POC, TC, and TIC were determined using the analyser TOC 5000-V-CPH (Shimadzu Co., Japan). The DOC in the water samples was determined using high-temperature (680°C) thermocatalytic oxidation. The TC content in SPM and sediment samples was determined using high-temperature (900 °C) combustion in airflow using an SSM 5000 A device. The total TIC content was determined by dry burning the samples at 200°C with H₃PO₄. The TOC content was determined as the difference between the TC and TIC contents in the samples. The error in the element measurements accounted for 1 rel. %. The reproducibility of the results was within ±5% (Lobus et al., 2015; Peresypkin et al., 2011).

Elemental analyses of the filtered water, SPM, and sediment samples was performed at the Analytical and Certification Center of the Institute of Microelectronic Technology and High Purity Materials (RAS). Inductively coupled plasma atomic emission spectrometry (ICP-AES) (ICAP-61, Thermo Jarrell Ash, USA) and inductively coupled plasma mass spectrometry (ICP-MS) (X-7, Thermo Elemental, USA) were used

for the elemental analyses of the filtered water samples and the solution obtained by the total dissolution of SPM and sediment samples in HNO₃ + HClO₄ (3:1 by volume, Merck) in an autoclave system (Ankon-AT-2, Russia). Karpov and Orlova (2008) and Orlova (2003) provided a detailed description of the autoclave digestion procedure. ICP-AES was used to measure the major (Na, Mg, P, S, K, Ca, Al, Ti, and Fe) and trace elements (Li, V, Cr, Mn, Co, Ni, Cu, Zn, and Sr). ICP-MS was only used for the analysis of trace elements (Li, Be, B, Sc, Cr, Ni, Cu, Zn, Ga, As, Se, Rb, Sr, Zr, Nb, Mo, Sn, Sb, Cs, Ba, Hf, W, Hg, Tl, Pb, Bi, Th, and U) and rare earth elements (REEs; Y, La, Ce, Pr, Nd, Sm, Eu, Gd, Tb, Dy, Ho, Er, Tm, Yb, and Lu). The combined use of ICP-AES and ICP-MS allowed for the comparison and validation of the measurements (of the six elements) performed by the two methods (Karandashev et al., 2008). The measurement error was not larger than 10–15 rel.% for ICP-AES and 10–30 rel.% for ICP-MS, in terms of the element content. In the results and discussion sections we discuss the most informative elements, while the remaining are given in the Tables 1–3 as reference material.

The grain size and mineralogy analyses were performed at the Analytical Laboratory of the Shirshov Institute of Oceanology (RAS). Grain size analyses of all the sediment samples were performed by wet sieving (Loring and Rantala, 1992). The mineral composition of the sediment samples (sts. 2, 4, and 7) was determined using an X-ray diffractometer (D8 ADVANCE, Bruker AXS, Canada) following previously proposed procedures (Moore and Reynolds, 1989).

2.3. Accuracy of the analytical determinations

The precision and validity of the analytical determinations were evaluated using certified reference materials (CRMs) that were randomly assigned. The following regulations were followed for using the CRMs: 'Trace Metals in Drinking Water' (European Union) for filtered water samples, Andesite, AGV-2 (United States Geological Survey), and Essexite Gabbro SRM-2A (Russian Geochemical Standard) for SPM and sediment samples. The discrepancy between the certified and measured element contents was within the limits of the confidence intervals in each case.

2.4. Calculation of the enrichment factor and partition coefficients

The enrichment factor (EF) was calculated as follows:

$$EF = [\text{Element}/\text{Al}]_{\text{Sample}} / [\text{Element}/\text{Al}]_{\text{Background}}$$

The average chemical composition of suspended particulate matter in World River SPM (WRSPM) and average chemical composition of World Shale values were used as the background for the SPM and sediments, respectively (Costa-Böddeker et al., 2017; Turekian and Wedepohl, 1961; Viers et al., 2009; Yao et al., 2016).

The partitioning coefficient $K_{\text{SPM/Water}}$ was calculated as the ratio of the element content in surface SPM and filtered water (Strady et al., 2017a; Turner et al., 1993). The partitioning coefficient $K_{\text{SPM/Sed}}$ was calculated as the ratio of element content in surface SPM and surface sediments (Koukina and Lobus, 2019).

2.5. Statistical analysis

Descriptive statistical analyses were computed using Microsoft Excel 2010 software. Pearson's correlation analysis was performed using SPSS 20.0 program. PCA was conducted using MATLAB R2018a computing environment (The Math Works, Inc., USA). RDA analysis was performed in MATLAB R2018a using the Fathom Toolbox (Jones, 2017). In all cases, PCA and RDA analyses were carried out on normalised data, that is, for every variable, its mean value was subtracted from the raw data, and then the obtained centred variables were normalised by their standard deviations.

Table 1

Major, trace and rare-earth elements in the surface water of the Cai River estuary.

Element	Salinity, ‰					WRDE ¹	WODE ²
	<0.01	8.49	15.82	33.12	33.56		
in g L⁻¹							
Na	0.01	0.54	1.51	10.71	10.87	0.005 ³	10.78
Mg	0.001	0.08	0.24	1.53	1.45	0.003 ³	1.28
K	0.002	0.02	0.07	0.47	0.45	0.001 ³	0.399
Ca	0.004	0.03	0.09	0.48	0.45	0.013 ³	0.412
in mg L⁻¹							
B	0.007	0.25	0.69	3.94	3.71	0.01	4.45
Si	6.97	6.16	5.29	0.26	0.27	4.85 ³	2.8
S	0.6	41.72	117.78	643.81	614.07	–	898
Br	0.04	5.02	15.05	91.70	85.14	0.02 ³	67
Sr	0.03	0.45	1.26	7.27	6.77	0.06	8.15
in µg L⁻¹							
Li	1.01	9.80	28.68	167.70	156.61	1.84	180
Al	137	23.8	< d/l	< d/l	< d/l	32	0.030
Ti	2.6	< d/l	< d/l	< d/l	< d/l	0.489	0.0065
V	0.54	< d/l	< d/l	< d/l	< d/l	0.71	2
Mn	1.9	25.3	23.9	< d/l	< d/l	34	0.020
Fe	127	74.8	< d/l	< d/l	< d/l	66	0.030
Cu	1.0	< d/l	< d/l	< d/l	< d/l	1.48	0.150
Zn	0.60	< d/l	< d/l	< d/l	< d/l	0.60	0.350
As	0.65	0.84	< d/l	< d/l	< d/l	0.62	1.2
Rb	6.52	13.38	26.83	122.01	114.05	1.63	120
Mo	0.20	0.92	2.15	11.17	10.90	0.42	10
Sn	0.49	0.50	0.30	1.39	< d/l	0.4 ³	0.0005
Sb	0.03	< d/l	< d/l	< d/l	< d/l	0.07	0.2
Cs	0.10	0.19	0.20	0.29	0.27	0.011	0.31
Ba	21.01	27.73	23.30	6.66	6.99	23	15
Pb	0.18	0.19	< d/l	< d/l	< d/l	0.079	0.0027
U	0.10	0.21	0.52	3.93	3.68	0.372	3.2
in ng L⁻¹							
Be	12.0	25.3	< d/l	< d/l	< d/l	8.9	0.21
Y	443	255	98.5	< d/l	< d/l	40	17
Zr	44.0	< d/l	< d/l	< d/l	< d/l	39	15
Nb	15.1	< d/l	< d/l	< d/l	< d/l	1.7	0.37
La	431	275	131	< d/l	< d/l	170	5.6
Ce	646	429	159	< d/l	< d/l	262	0.7
Pr	114	68.3	34.7	< d/l	< d/l	40	0.7
Nd	443	310	100	< d/l	< d/l	152	3.3
Sm	97.6	42.7	14.6	< d/l	< d/l	36	0.57
Eu	9.0	4.9	< d/l	< d/l	< d/l	9.8	0.17
Gd	95.8	48.3	27.3	< d/l	< d/l	40	0.9
Tb	14.4	9.4	2.1	< d/l	< d/l	5.5	0.17
Dy	77.3	50.9	15.8	< d/l	< d/l	30	1.1
Ho	18.2	9.9	5.4	< d/l	< d/l	7.1	0.36
Er	49.9	28.0	14.7	< d/l	< d/l	20	1.2
Tm	7.1	4.6	2.7	< d/l	< d/l	3.3	0.2
Yb	49.1	31.4	14.9	< d/l	< d/l	17	1.2
Lu	7.9	4.4	2.3	< d/l	< d/l	2.4	0.23
W	27.6	< d/l	< d/l	< d/l	< d/l	100	10
Tl	33.2	32.6	27.9	< d/l	< d/l	7	13
Bi	23.9	23.9	11	< d/l	< d/l	–	0.03
Th	94.4	31.0	< d/l	< d/l	< d/l	4.1	0.02

(1) – World average River Dissolved Elements (WRDE) by Gaillardet et al. (2014); (2) – World average Ocean Dissolved Elements (WODE) by Nozaki (2010); (3) – WRDE by Gordeev and Lisitzin (2014).

3. Results

3.1. Surface water and SPM characteristics

The water column of the Cai River estuary is highly stratified with pronounced horizontal and vertical salinity gradients (Koukina and Lobus, 2019). The salinity of the surface water layer within the sampling river-sea transect varied from 0 to 34‰, and the pH of the water column varied from neutral (pH 7) to low-alkaline (pH 8–9). Cai River water with a mineralisation of 40 mg l⁻¹ was collected upstream from the fill dam at sampling Site 1. Downstream from the dam, the salinity was 3‰ at Site 2, 8‰ at Site 3, 16‰ at Site 4, 25‰ at Site 5, and it increased to 33–34‰ at sites 6–8. The frontal zone was observed at sites 2–4, where the horizontal salinity gradient was as high as 3‰ per 1 km. The DOC concentration in the surface water layer varied within the range of

1.15–8.5 mg l⁻¹ and exhibited a maximum with salinities of 25‰ at Site 5 and 33‰ at Site 6 in the vicinity of the local marina (Fig. S1).

The TSS showed a maximum concentration of 50 mg l⁻¹ in the river water at Site 1 and showed an exponential decrease seaward with values of 33 mg l⁻¹ at 8.5‰ at Site 3, 11 mg l⁻¹ at 16‰ at Site 4, and 5 mg l⁻¹ at 25‰ at Site 5. The maximum concentration was the lowest (1–1.6 mg l⁻¹) at 33–34‰ downstream of sites 6–8. The POC generally followed the trend of the TSS distribution but exhibited a maximum concentration of 1.47 mg l⁻¹ downstream of the fill dam at 3‰ at Site 2, which then decreased to 0.94 mg l⁻¹ at 16‰ at Site 4, and then to 0.27 mg l⁻¹ at 25‰ at Site 5. The maximum concentration was the lowest (approximately 0.2 mg l⁻¹) at 33–34‰ downstream of sites 6–8.

Table 2

Major, trace and rare-earth elements in the surface SPM of the Cai River estuary.

Element	Stations								Mean ± SD	WRSPM ¹	WRSPM ²	
	1	2	3	4	5	6	7	8				
Major elements, in %												
Na	0.07	0.52	0.61	1.24	1.56	23.69	24.85	23.60	9.52 ± 12.04	0.71	0.71	
Mg	0.37	0.47	0.49	0.60	0.91	2.33	2.48	2.36	1.25 ± 0.95	1.26	0.58	
Al	15.11	15.21	15.41	14.62	9.81	1.40	1.30	0.78	9.21 ± 6.90	8.72	8.6	
P	0.08	0.10	0.11	0.14	0.14	0.14	0.15	0.11	0.12 ± 0.02	0.2	0.15	
K	1.00	1.10	1.20	1.35	1.39	1.60	1.61	1.40	1.33 ± 0.22	1.69	2.09	
Ca	0.31	0.24	0.16	0.16	0.63	0.80	0.83	0.82	0.49 ± 0.30	2.69	3.83	
Ti	0.18	0.17	0.15	0.12	0.10	0.03	0.03	0.02	0.10 ± 0.06	0.44	0.43	
Mn	0.07	0.05	0.04	0.03	0.04	0.04	0.05	0.05	0.05 ± 0.01	0.17	0.165	
Fe	4.67	4.71	4.77	5.31	4.90	0.99	0.45	0.25	3.26 ± 2.25	5.81	5.45	
Trace elements, in µg/g												
Li	57.09	60.11	60.32	57.37	32.96	10.21	9.50	8.67	37.03 ± 24.46	8.5	38	
Be	3.69	3.65	3.52	3.01	2.85	1.51	0.19	0.14	2.32 ± 1.50	–	1.7	
Sc	15.85	15.69	15.42	16.17	12.36	8.53	5.65	3.52	11.65 ± 5.08	18.2	15.9	
V	94.07	96.36	109.59	127.6	128.6	70.98	63.59	17.39	88.52 ± 37.15	129	149	
Cr	187.21	100.25	57.34	72.09	75.08	71.58	66.18	91.86	90.20 ± 41.53	130	137	
Co	175.41	125.69	13.66	12.24	12.29	30.25	60.91	116.96	68.43 ± 63.13	22.5	25	
Ni	384.24	289.61	52.48	61.56	59.52	88.95	119.56	171.2	153.39 ± 122.41	74.5	76	
Cu	201.66	116.47	31.6	34.25	30.96	103.89	119.16	201.11	104.89 ± 26.65	75.9	98	
Zn	116.07	117.89	119.56	103.54	84.39	33.52	28.00	35.87	79.85 ± 15.44	208	343	
Ga	38.34	36.85	36.94	35.54	21.85	8.11	2.77	2.09	22.81 ± 16.25	18.1	21	
As	42.42	39.11	34.88	39.85	45.36	30.25	6.61	89.64	41.02 ± 8.72	36.3	23.4	
Se	2.96	3.08	2.48	2.60	3.07	2.98	3.35	2.92	2.93 ± 0.28	–	1.75	
Rb	108.57	107.03	107.51	100.98	79.24	21.29	10.02	8.11	67.84 ± 46.41	78.5	93	
Sr	45.32	46.01	46.63	61.39	156.94	189.85	201.82	201.4	118.67 ± 75.04	187	173	
Zr	27.46	26.65	22.74	22.62	18.96	12.36	4.25	2.52	17.20 ± 9.74	160	164	
Nb	9.10	8.52	4.95	4.50	3.89	2.89	1.67	1.17	4.59 ± 2.92	13.5	13.7	
Mo	51.58	45.82	9.13	9.45	8.46	11.96	10.97	13.57	20.12 ± 17.78	2.98	8.7	
Ag	0.22	0.23	0.18	0.22	0.21	0.19	0.25	0.13	0.20 ± 0.04	–	0.3	
Cd	0.29	0.21	0.16	0.04	0.08	0.12	<d/1	<d/1	0.15 ± 0.09	1.55	3.2	
Sn	9.19	8.12	8.56	6.57	5.85	4.23	2.53	1.77	5.85 ± 2.79	4.57	4	
Sb	0.97	0.96	0.93	0.94	0.89	0.65	0.22	0.20	0.72 ± 0.33	2.19	2.2	
Cs	16.30	15.24	15.12	11.80	8.96	2.86	0.97	0.77	9.00 ± 6.63	6.25	6.4	
Ba	286.38	256.36	205.25	248.46	249.11	112.53	28.48	157.93	193.06 ± 87.73	522	547	
Hf	1.62	1.05	0.97	1.02	0.85	0.45	0.26	0.17	0.80 ± 0.48	4.04	4.6	
W	12.01	8.05	5.63	5.43	4.89	3.26	1.64	1.06	5.25 ± 3.55	1.99	1.58	
Ir	0.14	0.15	0.04	0.04	0.05	0.19	0.26	0.15	0.13 ± 0.08	–	–	
Hg	0.89	0.93	0.49	1.11	0.56	0.49	2.28	0.91	0.96 ± 0.58	–	0.104	
Tl	0.97	0.96	0.91	0.88	0.74	0.09	0.09	0.08	0.59 ± 0.42	0.53	0.62	
Pb	65.17	64.95	63.05	75.28	79.36	82.12	44.76	26.88	62.70 ± 18.63	61.1	89	
Bi	9.66	11.23	9.84	14.59	15.21	1.19	1.14	0.42	7.91 ± 6.13	0.85	0.43	
Th	49.44	48.85	45.82	40.41	34.13	5.21	4.17	2.54	28.82 ± 21.16	12.1	11	
U	9.08	10.21	10.33	8.77	5.56	0.89	0.49	0.43	5.72 ± 4.48	3.3	2.9	
Rare-earth elements, in µg/g												
Y	37.32	36.98	36.54	43.36	28.56	11.10	2.76	2.11	24.84 ± 16.84	21.9	26	
La	57.96	56.01	56.11	53.50	45.90	8.54	5.76	4.02	35.98 ± 25.02	37.4	37.9	
Ce	127.11	125.95	126.18	110.00	100.31	34.75	15.49	19.23	82.38 ± 50.19	73.6	72.4	
Pr	12.04	12.15	11.94	11.98	7.89	3.21	1.37	0.88	7.68 ± 5.10	7.95	–	
Nd	44.40	44.52	43.60	44.14	25.16	5.23	2.89	1.57	26.44 ± 20.29	32.2	36.2	
Sm	9.41	9.13	9.28	9.82	5.89	2.83	1.10	0.72	6.02 ± 3.94	6.12	6.5	
Eu	1.18	1.35	1.21	1.40	0.89	0.22	0.13	0.08	0.81 ± 0.57	1.29	1.4	
Gd	8.54	8.86	8.44	9.29	5.78	1.29	0.68	0.46	5.42 ± 3.96	5.25	4.8	
Tb	1.40	1.39	1.33	1.51	0.74	0.25	0.12	0.09	0.85 ± 0.63	0.82	1.03	
Dy	7.34	7.45	7.44	8.58	3.35	0.59	0.07	0.08	4.36 ± 3.74	4.25	3.8	
Ho	1.47	1.61	1.45	1.69	0.89	0.25	0.12	0.09	0.94 ± 0.70	0.88	–	
Er	4.31	4.48	4.15	4.94	2.98	1.11	0.33	0.27	2.82 ± 1.96	2.23	1.9	
Tm	0.61	0.55	0.58	0.69	0.41	0.09	0.05	0.03	0.38 ± 0.27	0.38	0.59	
Yb	3.85	3.93	3.69	4.46	2.89	0.85	0.19	0.20	2.51 ± 1.80	2.11	2.8	
Lu	0.58	0.52	0.55	0.66	0.39	0.11	0.04	0.03	0.36 ± 0.26	0.35	0.45	

(1) - Average Chemical Composition of World Rivers Suspended Particulate Matter (WRSPM) by Viers et al. (2009); (2) - WRSPM by Savenko (2006).

3.2. Surface sediment characteristics

Within the sampling river-sea transect of the Cai River estuary, the percentage of sand in the surface sediments decreased from 49% of the total dry weight at the river mouth to 2% in the bay (Site 8), constituting up to 71% at transitional Site 4. The silt content ranged from 24% to 48%, and this value showed an increasing trend at sites 5–6. The clay content ranged from 9% to 68%, and this value showed an increasing trend at sites 7–8. The surface sediments mainly contained quartz (37%–54% of the total dry weight), kaolinite (6%–15%), illite (10%–14%),

albite (7%–8%), gibbsite (4%–8%), clinochlore (3%–6%), and gypsum (1%–3%), which were present in each of the three selected samples (sites 2, 4, and 7). Orthoclase was present at sites 4 and 7 (10%). Microcline was present only upstream at site 2 (7%), whereas aragonite (2%) and calcite were only present in the bay sediment (Site 7).

The TOC content varied within the range 0.6–1.8%, whereas the TIC content was negligible and reached the range of 0.88–2.1% only in the bay (sites 7–8).

Table 3

Major, trace and rare-earth elements in the surface sediments of the Cai River estuary.

Element	Stations							Mean ± SD	World Shale ¹	WRSEd ²
	2	3	4	5	6	7	8			
Major elements, in %										
Na	2.45	2.82	1.28	1.50	1.81	1.27	2.14	1.90 ± 0.60	0.96	0.79
Mg	0.58	0.52	0.46	0.57	1.29	0.61	1.33	0.76 ± 0.38	1.50	0.57
Al	12.24	12.84	7.95	11.81	13.05	7.67	8.51	10.58 ± 2.42	8.00	4.3
P	0.06	0.05	0.03	0.05	0.05	0.04	0.05	0.05 ± 0.01	0.07	0.08
S	0.28	0.31	0.22	0.63	0.54	0.59	0.23	0.40 ± 0.18	0.24	0.02
K	1.58	1.57	1.93	1.87	1.69	1.69	1.93	1.75 ± 0.16	2.66	1.1
Ca	0.32	0.38	0.35	0.59	0.56	6.17	3.20	1.65 ± 2.24	1.60	1.7
Ti	0.39	0.37	0.25	0.41	0.39	0.34	0.40	0.37 ± 0.06	0.46	0.31
Mn	0.06	0.04	0.04	0.04	0.03	0.04	0.06	0.05 ± 0.01	0.085	0.05
Fe	4.51	4.53	2.46	4.30	4.22	3.66	4.15	3.98 ± 0.73	4.72	2.5
Trace elements, in µg/g										
Li	44.90	45.47	34.75	49.16	49.77	60.05	62.74	49.55 ± 9.50	66	20
Be	2.89	2.71	1.83	2.72	3.03	2.02	2.28	2.50 ± 0.46	3	1.5
Sc	15.22	14.72	8.16	15.11	14.90	11.01	12.56	13.09 ± 2.69	13	10
V	99.74	100.38	61.40	89.47	95.27	82.25	92.46	88.71 ± 13.56	130	50
Cr	45.80	47.69	27.93	41.40	42.80	53.93	66.73	46.61 ± 11.91	90	50
Co	9.38	7.81	4.93	8.97	8.68	8.98	12.17	8.70 ± 2.15	19	15
Ni	23.82	23.44	14.21	20.27	21.81	27.19	38.07	24.12 ± 7.34	68	25
Cu	21.80	21.01	13.42	16.94	20.42	12.09	18.21	17.70 ± 3.78	45	20
Zn	117.26	115.24	69.82	111.58	123.19	88.26	100.33	103.67 ± 18.96	95	60
Ga	29.43	29.72	17.37	27.63	29.97	17.60	19.02	24.39 ± 6.05	19	10
As	30.64	29.39	14.81	22.46	21.15	18.32	12.20	21.28 ± 6.93	13	6
Rb	144.77	141.42	148.53	159.43	158.57	142.59	154.52	149.97 ± 7.54	140	50
Sr	66.36	69.11	61.25	81.12	82.29	604.74	289.18	179.15 ± 204.51	300	150
Zr	87.93	84.01	61.75	103.59	91.63	85.16	74.61	84.10 ± 13.18	160	250
Nb	19.30	18.28	12.06	19.10	21.07	13.38	15.30	16.93 ± 3.37	11	20
Mo	5.06	3.68	2.10	2.74	4.03	0.57	0.51	2.67 ± 1.73	2.6	1.5
Ag	0.09	0.07	<d/l	0.09	0.09	<d/l	<d/l	0.09 ± 0.01	0.07	0.05
Cd	<d/l	0.15	<d/l	0.12	0.16	<d/l	<d/l	0.14 ± 0.02	0.3	0.4
Sn	7.61	6.51	4.14	5.98	6.23	3.73	5.44	5.66 ± 1.35	60	4
Sb	1.32	1.35	0.85	1.36	1.19	1.03	1.08	1.17 ± 0.19	1.5	2
Cs	13.05	12.46	7.91	11.53	12.63	9.15	9.50	10.89 ± 2.02	5	4
Ba	272.38	256.44	273.76	269.03	269.81	286.38	323.20	278.71 ± 21.49	580	290
Hf	2.80	2.85	2.43	3.41	3.71	2.57	2.14	2.84 ± 0.55	2.8	6
W	2.07	1.89	1.30	1.88	2.09	1.22	1.18	1.66 ± 0.41	1.8	5
Hg	0.05	0.05	0.04	0.04	0.02	0.02	0.03	0.04 ± 0.01	0.18	0.05
Tl	1.05	1.02	0.89	1.08	1.16	0.81	0.82	0.97 ± 0.13	1.4	1
Pb	60.64	60.18	39.43	59.82	71.56	35.12	44.10	52.98 ± 13.44	20	15
Bi	22.57	15.55	9.18	1.96	2.38	0.81	0.94	7.63 ± 8.56	0.43	0.2
Th	43.77	42.61	23.92	39.36	44.83	23.61	21.79	34.27 ± 10.60	12	10
U	8.00	6.69	4.48	7.76	8.32	5.27	3.87	6.34 ± 1.80	3.7	3
Rare-earth elements, in µg/g										
Y	34.65	30.78	19.47	36.07	38.32	18.79	18.06	28.02 ± 8.94	26	20
La	51.79	47.44	38.30	55.14	58.29	49.26	51.15	50.20 ± 6.37	32	38
Ce	118.63	114.86	89.78	127.66	141.87	112.29	112.94	116.86 ± 15.91	70	75
Pr	11.75	10.77	8.70	12.83	13.38	10.94	11.14	11.36 ± 1.53	7.9	8
Nd	45.78	41.95	32.82	51.01	51.19	41.60	42.84	43.88 ± 6.33	31	30
Sm	9.33	8.42	5.96	10.33	10.48	7.53	7.74	8.54 ± 1.63	5.7	6
Eu	1.25	1.11	0.86	1.35	1.37	1.21	1.38	1.22 ± 0.19	1.2	1.5
Gd	8.24	7.33	4.85	8.94	8.98	5.81	5.75	7.13 ± 1.67	5.2	6
Tb	1.21	1.10	0.70	1.25	1.39	0.83	0.82	1.04 ± 0.26	0.85	1
Dy	6.93	6.23	3.96	7.13	7.66	4.19	4.08	5.74 ± 1.61	4	5
Ho	1.36	1.24	0.78	1.42	1.55	0.80	0.77	1.13 ± 0.34	1.04	1
Er	3.93	3.55	2.24	4.06	4.40	2.24	2.17	3.23 ± 0.98	3.4	3
Tm	0.57	0.51	0.34	0.58	0.63	0.33	0.33	0.47 ± 0.13	0.5	0.5
Yb	3.79	3.50	2.22	3.92	4.20	2.18	2.04	3.12 ± 0.94	3.1	3
Lu	0.54	0.49	0.32	0.57	0.61	0.30	0.30	0.45 ± 0.14	0.48	0.4

(1) - Average Chemical Composition of World Shale by [Turekian and Wedepohl \(1961\)](#); (2) - Average Chemical Composition of World Rivers Sediments (WRSEd) by [Savenko \(2006\)](#).

3.3. Element enrichment and distribution

3.3.1. Filtered (dissolved) elements

The baseline bulk concentrations of major and trace elements, and REEs in the surface water along the Cai River estuary are presented in [Table 1](#). The Cai River water generally contained higher amounts of Al, Ti, Fe, Y, Nb, Tl, Pb, Th, and REEs (except Eu) with respect to the World average River Dissolved Elements (WRDE). Trace metal contents at all the sampling sites did not exceed the recommended levels for irrigation water ([WHO, 2006](#)) and the maximum permitted value for protecting

aquatic life ([US EPA, 2006](#)). According to the available regional data, the concentrations of potentially toxic elements (Pb, Cu, Zn, and As) were lower than the average concentrations in the urban Nhue, To Lich, and Saigon rivers, and Mekong Delta waters in Vietnam ([Costa-Böddeker et al., 2017; Cuong et al., 2019; Strady et al., 2017a, 2017b, 2017b; Thanh-Nho et al., 2018; Thuong et al., 2015](#)).

Most of the elements studied were detected only at the upstream sites, whereas Si, Ba, Li, B, Na, Mg, S, K, Br, Sr, Rb, Mo, Cs, and U were detected at all the sites along the river-sea transect. To analyse element behaviour at estuarine gradients, PCA was applied to evaluate the

element concentrations along with selected environmental factors (salinity, TSS, and DOC) (Tables S1–S2). The spatial distribution of the dissolved elements was found to be mainly associated with axis 1 (PC 1, 97%), which is close to the salinity gradient. Li, B, Na, Mg, S, K, Br, Sr, Rb, Mo, Cs, and U were found to be strongly positively associated with salinity and were most abundant in the bay water (sites 7–8). All these elements are related to the major and minor constituents of seawater that show a conservative (that is, follow salinity) type of oceanic distribution and originate from global processes releasing these elements into the dissolved load (Gaillardet et al., 2014; Nozaki, 2010). Si and Ba, along with DOC and TSS, were strongly negatively associated with salinity and were most abundant in the river water (Site 1). Both Si and Ba show moderate chemical mobility in erosion, weathering, transport processes, and a recycled (nutrient-like) oceanic distribution when involved in biological uptake in surface water (Dyrssen, 2010; Gaillardet et al., 2014). The dissolved forms of these elements originate from silicate weathering of the basement Paleo-Mesozoic felsic intrusive rocks under warm and humid tropical climatic conditions (Sang et al., 2019).

The PCA revealed that upstream sites 1, 3, and 4 were clearly separated from downstream sites 7 and 8. Such a separation indicates that the dissolved loads of major and trace elements were significantly modified within the estuarine water-mixing zone (Guinoiseau et al., 2016). Thus, some elements (such as Si and Ba) were removed from the solution and there was a global TSS loss in the frontal end of the mixing zone, whereas the other elements (such as Li, B, Na, Mg, S, K, Br, Sr, Rb, Mo, Cs, and U) could be effectively transferred across the estuarine gradients.

3.3.2. Particulate elements

The baseline bulk concentrations of major and trace elements and REEs in SPM along the Cai River estuary are presented in Table 2. The mean contents of most major and trace elements, and REEs in the SPM from the Cai River estuary and Nha Trang Bay corresponded to the average WRSPM (World Rivers Suspended Particulate Matter), whereas Co, Ni, Cu, As, Mo, W, Pb, Bi, Th, and U exceeded the reference values.

To compare the results from different elements with drastically different abundances and to specify the potential risk elements, the data were introduced in the form of the EF (enrichment factor) calculated as doubly normalised to the bulk Al content (Viers et al., 2009; Suja et al., 2018). In surface SPM, Na showed the highest enrichment factor in the downstream SPM, most probably due to the ion exchange with the seawater solution. As per risk elements, Bi, Co, and Mo showed the highest average EF of 9, 12, and 16, respectively, followed by Li, Mg, Ni, Cu, and As (average EF 4–6), then by Li, K, V, Cr, Sr, Sn, Ba, W, and Pb

(average EF 2–3), while the EF of other elements studied did not exceed 1.

To trace element source and mobility at the estuarine gradients, the enrichment factor along with selected environmental factors (salinity, TSS, and POC) were subjected to PCA. The first two PCA axes accounted for 89% of the total variation (Tables S3–S7). The PCA plot in Fig. 2a shows the strongest element relationships, which can be interpreted as multi-element signatures in the surface SPM.

The first of the highlighted element groups included Fe, Cs, Y, and heavy, HREEs (Lu, Yb, Tm, Er, Ho, and Gd). The EF of these elements showed a strong positive correlation with each other ($r = 0.81\text{--}0.95$) and a positive association with axis 2 (PC 2), which may indicate their association with the iron oxyhydroxide fraction of the fluvial colloid pool (Turner et al., 1993). The mobility of these elements within the particulate phase is therefore mainly regulated by processes such as aggregation/degradation of colloids and sorption onto/desorption from colloids, which largely occur within the water mixing zone (Gaillardet et al., 2014). Earlier, the laboratory mixing experiments of Johannesson et al. (2017) showed that the fractionation behaviour of the REEs in the mixing zones was mainly controlled by salt-induced flocculation and coagulation of Fe-rich organic colloids.

The second group included Zr, Rb, and REEs (Tb, Eu, Sm, and Pr). The EF of these elements was strongly positively correlated with each other ($r = 0.95\text{--}0.99$), and with the EF of Ho. The third group included Ti, Sn, Sb, Sc, Pb, V, W and light, LREEs (Ce and La). The EF of these elements were strongly positively correlated with each other ($r = 0.88\text{--}0.98$) and positively linked to salinity and POC. Owing to the strong relationship between Zr and Ti, terrigenous detrital heavy minerals such as zircon and titanite may be the major source of the respective element groups. The EF of these elements was also mainly positively associated with axis 1 (PC 1), which represents the mineralogical and grain size fractionation of the riverine particulate load along the salinity gradient. This is consistent with a previous study (Kaotekwar et al., 2019), that attributed trace and REE fractionation to the preferential enrichment of specific element-bearing minerals (zircon and titanite in particular) in different grain size fractions of sediments from the lower Krishna River. Nonetheless, sorption onto organic colloids may also contribute to LREE enrichment within the particulate phase due to the positive association with POC.

Within the first three element groups, REEs tend to rank/fractionate from light (La) to heavy (Lu) following the gradient of principal component 2 (PC 2), which is attributed to the salt-induced flocculation and coagulation of riverine colloids. According to Sholkovitz and Szymczak (2000), fractionation of REEs in estuaries occurs during both

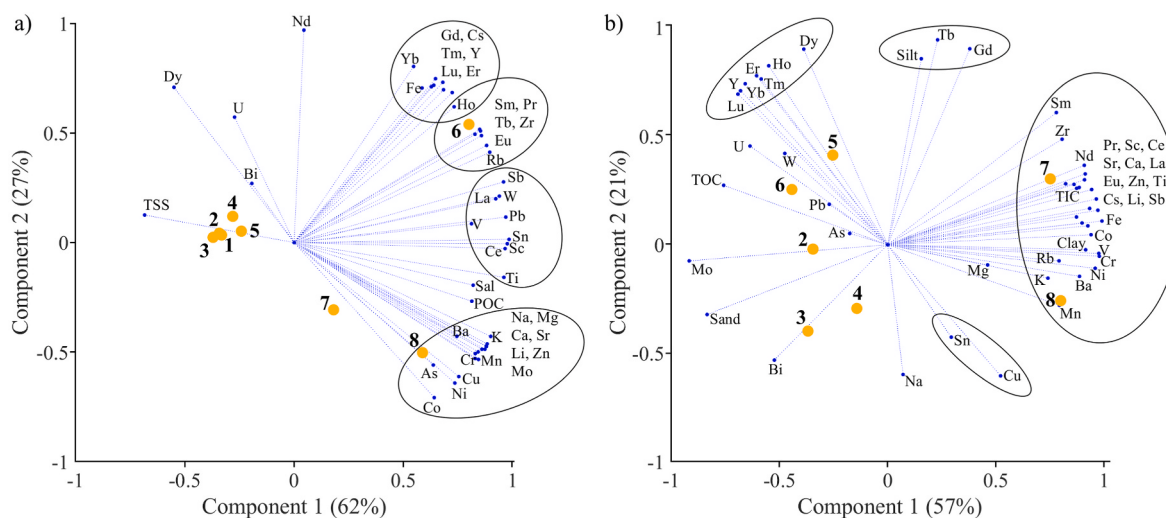


Fig. 2. PCA plot for the enrichment factors of SPM (EF_{SPM}) (a); PCA plot for the enrichment factors of the sediments (EF_{Sed}) (b).

removal and release from solution, leading to the preferential removal of LREEs and the preferential release of HREEs during estuarine mixing. At the same time, Viers et al. (2009) established that REE fractionation in suspended sediments occurs in environments where physical weathering is strongly dominant over chemical weathering. Therefore, physical weathering of Paleo-Mesozoic felsic intrusive rocks enhanced by intensive monsoonal precipitation and extreme climatic events may largely contribute to REE fractionation in the Cai River suspended load (Giuliani et al., 2019).

The fourth group included Li, Na, Mg, K, Ca, Co, Ni, Cu, Zn, Sr, Mo, Cr, Mn, Ba, and As. The EF of these elements were strongly positively correlated with each other ($r = 0.82\text{--}0.99$), mainly positively associated with axis 1 (PC 1), positively correlated with salinity and POC, and negatively associated with TSS. These elements exhibited a pronounced increase in the EF in SPM along the salinity gradient due to adsorption and/or substitution on the clay lattice, association with the organic colloids, and calcium carbonate (Suja et al., 2017; Dyrssen, 2010). This element group, including the risk elements Co, Mo, Ni, Cu, and As (EF 6–16), exhibited the highest efficiency of their transfer across the estuarine gradients, which may pose a risk to the coastal environment.

Outside the highlighted element groups, the EF of Dy, Nd, and U were positively correlated to axis 2 (PC 2), which may indicate their association with the fluvial colloid pool. In contrast to the other risk elements, Bi was not associated with any element or axis considered, which may indicate a distinctive (possibly non-weathering) source of this element.

The PCA results clearly separated the estuarine sites 1–5 from the marine sites 6–8. In contrast to the dissolved elements, the EF distribution of particulate elements showed a similarity within the group in upstream sites 1–5, whereas the group in the downstream sites followed the gradient of principal component 2 (PC 2) according to estuarine colloid dynamics (Sholkovitz and Szymczak, 2000). Such a separation can be explained with the concept of an estuarine geochemical filter that induces the major transformation of fluvial particulate element fluxes. Thus, particulate Fe, Ti, and Zr, along with associated trace elements and REEs, tend to accumulate within the transitional zone along with a global TSS loss, whereas risk elements such as Co, Mo, Ni, Cu, and As may be transferred across estuarine gradients and concentrate within the particulate phase in the bay.

3.3.3. Sedimentary elements

The bulk concentrations of major and trace elements, and REEs in the surface sediments (SPM) along the Cai River estuary are presented in Table 3. The mean content of most of these elements in the sediments of the Cai River estuary and Nha Trang Bay corresponded to World Shale and the average World Riverbed Sediments (WRSe), whereas the mean content of Pb, Th, U, and especially Bi, significantly exceeded the reference values.

To weigh the results from contrast element abundances and to identify the potential risk elements, the data were introduced in the form of an EF (Barats et al., 2020; Costa-Böddeker et al., 2017). In surface sediments, Bi showed the highest EF variability among the elements studied (EF range 2–34), with an exponential decrease from the river to the sea. These values are much higher than the respective EF range of Bi reported by Tran et al. (2018) for surface sediments of the Cau Hai Lagoon of Central Vietnam. Although these authors indicated moderate to severe Bi enrichment (EF 5–10), Bi in their study was considered a nontoxic element that does not constitute a real threat to the environment. In addition to Bi, Pb in this study also showed a heightened but constant EF along the salinity gradient (EF ~2), which corresponded to our previous estimate (Koukina et al., 2017). For the other elements studied, EF did not exceed the threshold value of 1.5 (Grygar and Popelka, 2016).

PCA was implemented to ordinate the elements according to their mobility in transferring across the estuarine gradients and to their affinity to selected environmental factors (salinity, TOC, TIC, and grain

size). The first two PCA axes accounted for 78% of the total variation (Tables S8–S12). The PCA plot in Fig. 2b shows the strongest element relationships which can be interpreted as multi-element signatures in surface sediments.

The largest element association comprised Li, K, Ca, Sc, Ti, V, Cr, Mn, Fe, Co, Ni, Rb, Sr, Zr, Zn, Sb, Cs, Ba, and LREEs (La, Ce, Pr, Nd, Sm, and Eu). The EFs of these elements were mainly strongly positively linked to each other and to axis 1 (PC 1) ($r = 0.80\text{--}0.99$) exhibiting the most pronounced enrichment at bay sites 7 and 8. Because of the strong positive association with the clay and carbonate (TIC) content, the main source of these elements may be fine-grained terrigenous aluminosilicate clay minerals (such as kaolinite, illite, and clinochlore) along with carbonates (such as calcite and aragonite). The strong affinity of major and trace elements, and REEs to sedimentary clay fractions in tropical rivers has been discussed in several recent studies. Kaotekwar et al. (2019) showed an increase in LREEs in clay fractions in the Krishna River sediments (India) due to the adsorption and/or substitution on clay lattice. In a study by Prabakaran et al. (2019), most of the major and trace elements, and REEs were found to be associated with clays in the Baram River sediments (Borneo). Within this group, the EF of K and Rb were strongly positively correlated with each other ($r = 0.99$), indicating similar mineralogical sources of these elements as Rb easily substitutes K in crystal lattices (Savenko, 2006). Outside this group, the EF of Mg showed some affinity to the clay content.

The second group consisted of two REEs, Gd and Tb, which were strongly positively linked to each other ($r = 0.94$) and the silt fraction ($r = 0.80$), and positively associated with axis 2 (PC 2). The main factor controlling the distribution of Gd and Tb in surface sediments may be the differential settling of Cd-Tb-bearing silt-sized material at sites determined by estuarine hydrodynamics (Koukina and Lobus, 2020; Lasareva et al., 2019). Kaotekwar et al. (2019) showed that grain size sorting and mineral differentiation of solid fluvial discharge may cause accumulation of various minerals in different size fractions, resulting in variations in their REE and trace element compositions.

The third group comprised the most of heavy REEs (Y, Dy, Ho, Er, Tm, Yb, and Lu) that were strongly positively linked to each other ($r = 0.95\text{--}0.99$) and positively linked to axis 2 ($r = 0.71\text{--}0.92$). The EF of these elements tended to decrease seaward but exhibited the most pronounced enrichment at intermediate sites 5 and 6. The main source of these elements may be the HREE-bearing terrigenous detrital heavy minerals. This is consistent with the study results reported by Prabakaran et al. (2019), who found that HREE (Ho, Er, Tm, Yb, and Lu) distribution was related to the sorting of heavy minerals owing to the recycling of source sediments in the tropical Baram River.

Within the three element groups, REEs tend to rank/fractionate from light (La) to heavy (Lu), along with grain size and salinity. Therefore, the major factors controlling REE enrichment and distribution in the surface sediments are grain size sorting and mineralogical fractionation of the solid fluvial load at the estuarine gradients.

Outside the highlighted element groups, the EF of Mo was strongly negatively associated with axis 1 ($r = -0.90$) and strongly positively linked to sand content ($r = 0.85$). The EF of Bi was positively associated with Mo ($r = 0.75$), whereas both Mo and Bi showed a pronounced enrichment at the upstream sites 2–4. Therefore, the coarsest sand-sized terrigenous material is a major source of Mo and Bi in estuarine sediments. The EF of Pb and As were negatively associated with each other ($r = -0.77$), which may be due to the increase in pH along the salinity gradient. In the study of the Karstic River system (China) by Li et al. (2018), Pb showed a higher affinity for solid materials when the pH values increased, whereas As was released into the water column when pH values were alkaline. The EF values of W and U were mainly positively associated to the elements of HREE group, while U was also strongly positively correlated to TOC ($r = 0.97$). The EF values of Cu and Sn were strongly and positively linked to each other ($r = 0.85$). Both Cu and Sn exhibited a maximum enrichment at bay Site 8, which may be conditioned by the presence of traces of Cu-Sn intermetallic minerals

(Xie et al., 2006). Since no smelting or refining of base metals has officially been reported in the catchment area of the Cai River, local mining operations have to be considered.

The PCA results clearly separated upstream sites 2–6 from downstream sites 7–8 due to the global transformation of sedimentary material at the estuarine gradients. Thus, the sand- and silt-sized riverine material enriched in Bi, Mo, and HREEs is preferentially deposited within the transitional zone (sites 2–6), whereas the most fine-grained material enriched in clays, carbonates, and most of the trace and LREEs was transferred across the estuarine geochemical filter and accumulated within the sedimentary phase in the bay (sites 7–8).

4. Discussion

4.1. Processes controlling filtered/particulate phase distribution

To compare the results from the filtered and particulate phases, the partitioning coefficient $K_{\text{SPM/Water}}$ (or K_d) was calculated as the ratio of particulate-to-filtered element concentrations, illustrating the distribution of elements between dissolved and particulate phases in the surface water layer (Thanh-Nho et al., 2018; Thuong et al., 2015; Turner et al., 1993; Tomczak et al., 2019).

PCA was used to reveal the partitioning patterns at the estuarine gradients, and it was found that the $K_{\text{SPM/Water}}$ of the elements detected along the river-sea transect are related to the selected environmental factors (such as salinity, TSS, and organic carbon) (Tables S13–S14). The key results showed that the particulate form was strongly dominant for all elements at the river mouth. The $K_{\text{SPM/Water}}$ of Rb, Cs, and U were strongly positively linked to TSS ($r = 0.95\text{--}0.99$), positively linked to OC (calculated as the ratio of POC to DOC), and strongly negatively linked to salinity ($r = -0.94$ to -0.96). These elements were mainly accumulated within the particulate phase upstream (at 0–16%). The $K_{\text{SPM/Water}}$ of Na, K, Ca, Mg, Sr, Li, and Mo were found to be strongly positively linked to each other ($r = 0.98\text{--}0.99$), positively associated with TSS, and negatively linked to the salinity gradient. These elements are most mobile within the estuary and are dominantly accumulated within the dissolved phase downstream.

PCA also revealed that river Site 1 was clearly separated from transitional and bay sites 3–8. The distribution of the values of $K_{\text{SPM/Water}}$ indicates a global element transition from the particulate phase, characteristic of a freshwater environment, to the dissolved phase, which is dominant in the ocean, whereas the estuarine water mixing zone acts as a selective geochemical filter for the dissolved fluvial load. The site separation effect was largely enhanced by the fill dam located between sites 1 and 2.

4.2. Processes controlling particulate/sedimentary phase distribution

The partitioning coefficient $K_{\text{SPM/Sed}}$ was used to compare the results from the particulate and sedimentary phases. The $K_{\text{SPM/Sed}}$ was first introduced in our previous work and was calculated as the ratio of the element content in surface SPM and surface sediment (Koukina and Lobus, 2019). In this work, $K_{\text{SPM/Sed}}$ was used to reveal associations between elements that are characterised by similar fractionation patterns at the estuarine gradients. The average $K_{\text{SPM/Sed}}$ of Ti, Zr, Rb, and Pb was much lower than 1 (0.2–0.4), indicating their primary accumulation within the sedimentary phase. The average $K_{\text{SPM/Sed}}$ of Li, Al, K, Ca, Sc, V, Mn, Fe, Zn, Sr, Sn, Sb, Cs, Ba, Pb, U, and REEs were less than or approximately 1, being generally similarly abundant in both sediments and the SPM phase, which indicates clays as their host minerals because clay minerals are the major constituents of both SPM and sediments (Gaillardet et al., 2014; Savenko, 2006). Mo (average $K_{\text{SPM/Sed}} = 10$), Co, Cu, and Ni (average $K_{\text{SPM/Sed}} = 5\text{--}6$), Cr, W, As, and Bi (average $K_{\text{SPM/Sed}} = 2\text{--}3$) were primarily concentrated in the particulate phase. Along the salinity gradient, the $K_{\text{SPM/Sed}}$ of most elements studied tended to decrease from the river to the sea, exhibiting a maximum at an

intermediate salinity of 16‰ at Site 4.

PCA approach was applied to ordinate the elements according to their partitioning patterns and affinity to environmental factors (salinity, TSS, and organic carbon) (Tables S15–S19). The first two PCA axes accounted for 82% of the total variation. The PCA plot in Fig. 3a shows the strongest element relationships in relation to the partitioning patterns between solid phases.

The $K_{\text{SPM/Sed}}$ of Na, Mg, and K, were positively linked to each other (0.83–0.87). As major constituents of seawater, Na, K, and Mg are primarily accumulated within the particulate phase downstream owing to the free ion uptake from the seawater solution.

The largest of the highlighted element groups comprised Li, Al, Sc, Ti, Fe, Zn, Rb, Zr, Cs, Sn, Sb, W, U, and Y along with REEs. The $K_{\text{SPM/Sed}}$ of these elements were strongly positively linked to each other ($r = 0.76\text{--}0.99$) and strongly positively associated with axis 1 (PC 1) ($r = 0.94\text{--}0.99$), which was, in turn, positively loaded with the transitional sites 2–4. The $K_{\text{SPM/Sed}}$ of Ba, Pb, V, and Cr were mainly positively associated to these elements, while V and Pb were strongly positively correlated to each other ($r = 0.92$). Within this group, the partitioning patterns of trace elements and REEs were strongly linked to the major elements Al and Fe which are recognised as proxies of terrigenous aluminosilicates and Fe-oxyhydroxides (Koukina et al., 2017). Therefore, adsorption/substitution on clay lattices and association with Fe-oxyhydroxides mainly control trace and REE abundances in both solid phases. The partitioning between solid phases is largely conditioned by flocculation, coagulation, and further sedimentation of the fluvial clays and Fe colloids induced by a salinity increase. This is consistent with the study of Costa-Böddeker et al. (2017), which highlighted the crucial role of the salinity gradient in metal partitioning in the Thi Vai estuary in south-eastern Vietnam.

The $K_{\text{SPM/Sed}}$ values of Ca and Sr were strongly positively linked to each other ($r = 0.92$) and negatively associated with axis 2 (PC 2). Sr is enriched in carbonate rocks because of its similar ion radius to Ca (Li et al., 2018), and the partitioning of both Ca and Sr between the solid phases is therefore mainly conditioned by fluvial carbonate (such as calcite and aragonite) supply and/or biogenic carbonate formation. The $K_{\text{SPM/Sed}}$ of Mn was positively associated with axis 2 because of the affinity to carbonates. The $K_{\text{SPM/Sed}}$ of organic carbon (OC, calculated as the ratio of POC to TOC) increased seaward, exhibiting a maximum at downstream sites 7–8, most probably due to plankton growth.

Among the highlighted risk elements, Co, Ni, Cu, and Mo showed similar partition patterns, preferentially accumulating within the particulate phase in the bay. The $K_{\text{SPM/Sed}}$ of Co and Ni, Cu and Mo were strongly positively associated pairwise ($r = 0.85$ and 0.94 , respectively). The $K_{\text{SPM/Sed}}$ Cu and Mo were also positively linked to the $K_{\text{SPM/Sed}}$ of OC because of their affinity to organic matter. The $K_{\text{SPM/Sed}}$ values of As and Bi were not linked to any element or environmental factors that were considered. For both Bi and As, a possible non-weathering input should be specified.

The PCA results for the $K_{\text{SPM/Sed}}$ data confirmed that the upstream sites 2–5 were clearly separated from downstream sites 6–8. Such a separation indicates a global TSS loss induced by the large-scale sedimentation of riverine particulate materials when the salinity initially increases (0–16‰), followed by the accumulation of major elements, trace elements, and REEs in the sedimentary phase downstream (25–34‰). However, risk elements such as Co, Ni, Cu, and Mo were effectively transferred across the estuarine gradients and preferentially accumulate within the particulate phase in the bay.

To identify the relationship between the elements investigated in this study and the most significant environmental variables determined using PCA, RDA (redundancy analysis) was applied to the $K_{\text{SPM/Sed}}$ dataset. The results of the PCA analysis showed that most of the variance in the $K_{\text{SPM/Sed}}$ dataset can be explained using two or three principal components, suggesting that the dataset is highly redundant and its dimensionality can be significantly reduced (Legendre, 2019). To evaluate the redundancy of the dataset, we performed RDA using three

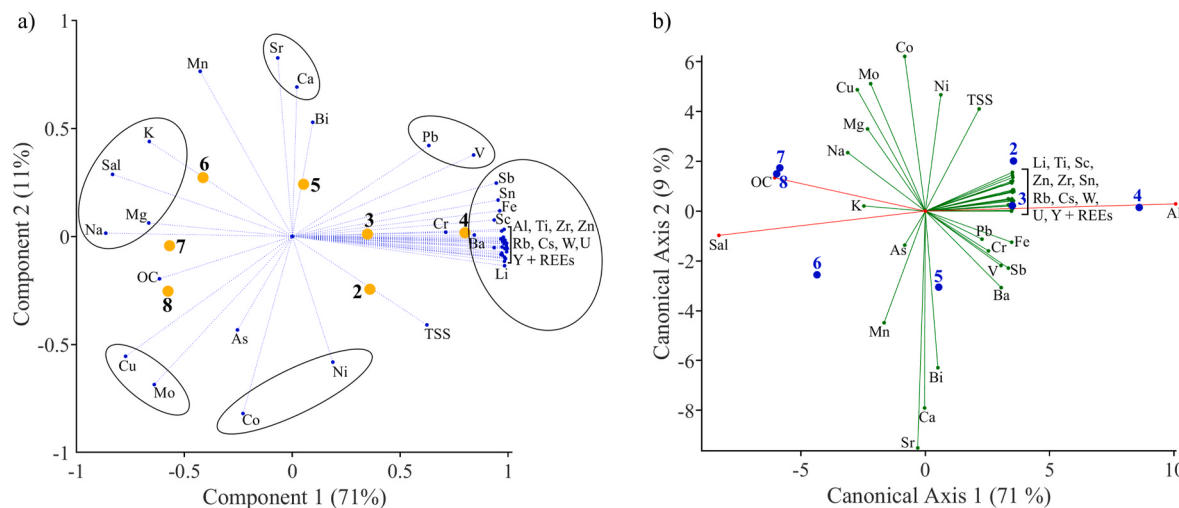


Fig. 3. PCA plot for the partitioning coefficient ($K_{\text{SPM/Sed}}$) (a); RDA plot for the partitioning coefficient ($K_{\text{SPM/Sed}}$) (b).

explanatory variables: (1) surface water layer salinity as the marker of salinity gradient, (2) $K_{\text{SPM/Sed}}$ for Al as the proxy for terrigenous clay minerals, and (3) $K_{\text{SPM/Sed}}$ for OC calculated as the ratio of POC to TOC, reflecting the organic matter distribution. Overall, the results of the RDA, presented in Fig. 3b, revealed that the three explanatory variables are, in fact, sufficient to explain most (87%) of the variance in the dataset. The angle between the $K_{\text{SPM/Sed}}$ of the elements and the environmental variables that were considered reflected their relevance (Huang et al., 2020). The projection of the sites (2–8) onto the environmental variable vector reflected the variable load on the site. The RDA plot in Fig. 3b shows the strongest relationships in relation to the explanatory variables.

Based on the RDA results, a large group of elements (Li, Ti, Sc, Cs, Rb, Zr, Zn, Sn, W, U, Y, and REEs) that were strongly relevant for Al, were clearly separated from the rest of the elements investigated. Therefore, it was found that the fractionation of these elements between the particulate and sedimentary phases along the salinity gradient is mainly controlled by their association with terrigenous aluminosilicate clay host minerals. The main host minerals are kaolinite, illite, and clinochlore, which constitute the fine-grained fraction of sedimentary materials. A study by Sang et al. (2019) showed that kaolinite in central Vietnam shelf sediments originated from the chemical weathering of Paleo-Mesozoic felsic intrusive rocks under warm and humid climate conditions, whereas illite was mainly derived from the physical weathering of Paleo-Mesozoic felsic intrusive rocks and Precambrian metamorphic rocks. These elements enter the estuary within the suspended particulate load of the fluvial discharge and are largely accumulated within the particulate phase in the frontal and transitional zones (at 3–16%) due to the slowing of the river flow at the fill dam and to the coagulation of riverine colloids induced by the salinity rise. Finer particles and high Al concentrations in SPM resulted in higher trace element concentrations (Fernandes et al., 2019). The fine-grained clay-rich suspended material is deposited during the homogenisation of the water column in the sea floor depression, where Li, Ti, Sc, Cs, Rb, Zr, Zn, Sn, W, U, Y, and REEs accumulate within the sedimentary phase (Iglesias et al., 2020). V, Cr, Fe, Ba, and Sb, and, to a lesser extent Pb, were also positively associated with Al and the elements of the first group, but were primarily accumulated within the particulate phase in the transitional zone (at 16–25%), most probably due to the association with Fe-colloids (Prabakaran et al., 2019).

Na, Mg, and K are primarily accumulated within the sedimentary phase upstream due to the deposition of coarse fluvial suspended sediments containing Na-, K-, and Mg-bearing detrital minerals (such as albite and microcline) and within the particulate phase downstream due to the uptake from the solution, as these elements are the major

constituents of seawater. Ca and Sr, and to a lesser extent Mn, were not associated with explanatory variables, being primarily accumulated within the sedimentary phase in the bay at 33–34% due to their association with carbonate minerals (calcite, aragonite).

OC largely explained the variance of Cu and Mo that were mostly accumulated within the particulate phase downstream, most probably because of their association with organic matter of autochthonous and/or terrigenous origin (Lobus et al., 2015; Peresypkin et al., 2011). Co and Ni were not associated with the selected environmental variables and were primarily accumulated within the particulate phase at the river mouth at the initial salinity rise of 0–3% and the highest TSS. Co, Ni, Cu, As, and Mo were also largely accumulated within the particulate phase at the furthest downstream site at 34%. Generally, Co, Ni, Cu, As, and Mo showed the highest chemical mobility due to their association with the most labile fraction of the fluvial particulate load (mainly clay, organic colloids, and carbonate).

Bi showed a distinctive distribution and partition pattern that was not associated with the explanatory or other variables considered. Bi was mainly accumulated within the upstream sediments and also showed a pronounced enrichment peak in the particulate phase at a transitional salinity of 16%. Because Bi settles within the sedimentary phase upstream, the major source of Bi within the estuary has to be the coarsest fluvial material that is deposited at the river mouth (Koukina et al., 2017). Although metallic Bi is not considered toxic (Tran et al., 2018), the source of Bi in the upstream areas and watershed of the Cai River flow should be further investigated. Bismuth is a by-product of lead refining (Ojebuoboh, 1992). In Vietnam, bismuth has been found in the tin, lead-zinc, and tungsten deposits of hydrothermal and skarn origin that are widespread in the north of the country (Khoi, 2014). Since no smelting or refining of base metals has officially been reported in the catchment area of the Cai River, local mining operations have to be considered as Vietnam has recently become a leading producer of Bi worldwide, making 2000 tons of it per year (Naumov, 2007).

Generally, the RDA results confirmed the separation of upstream sites 2–5 from downstream sites 6–8 in relation to the geochemical composition of the solid phases. This contributes to the concept of an estuarine geochemical filter that induces a global transition from the terrigenous to aquagenous geochemical composition of the solid phases.

5. Conclusions

This study provides baseline concentrations of filtered, particulate, and sedimentary elements (major and trace, and REEs) along with surface water (salinity, TSS, DOC, and POC) and surface sediment (mineralogy, granulometry, TOC, and TIC) characteristics in the tropical

Cai River estuary under multiple stresses.

The application of the PCA and RDA to the data comprising EF and partitioning coefficients, $K_{\text{SPM/Water}}$ and $K_{\text{SPM/Sed}}$, highlighted the strongest element relationships, considered as multi-element signatures in solid and solution phases, and revealed the main fractionation patterns along the salinity gradient in the stratified Cai River estuary. Generally, element distribution, mobility, and partitioning are mainly controlled by the estuarine hydrodynamics and are largely associated with the differential settling of fluvial mineral element-bearing phases, while further studies should focus on the composition and dynamics of colloid pools.

Based on results of the aforementioned analyses, the elements were ranked according to the efficiency of their transfer across the estuarine gradients. Thus, most of the major and trace elements, and REEs investigated in this study showed low chemical mobility and mainly settle in the downstream sedimentary phase due to their association with terrigenous aluminosilicate clay host minerals. In contrast, the highlighted risk elements, Co, Ni, Cu, As, and Mo, were largely accumulated in downstream particulate phases and showed high chemical mobility and efficiency of transfer across estuarine geochemical filter owing to their association with the most labile fraction of the fluvial particulate load (such as clays, organic colloids, and carbonates). Most of the elements were introduced in the Cai River and its estuary by basement rock weathering under enhanced monsoonal precipitation, whereas Bi showed both severe enrichment and a non-weathering distribution pattern in the solid phases. The source of Bi in the upstream areas and watershed of the Cai River flow should be further investigated with special attention to mining activity in the region.

This study has effectively linked element associations to environmental factors along a small tropical estuary. Notably, the application of PCA and RDA to $K_{\text{SPM/Sed}}$ has proved to be an efficient tool for ranking elements according to their mobility and fractionation within the estuarine geochemical filter. This suggests a relevance/applicability of the method used to the other high-gradient zones. However, the implemented multivariate approach needs further elaboration.

Funding information

This research was performed within the framework of the state assignment of Shirshov Institute of Oceanology, Russian Academy of Sciences (IO RAS) (theme no. 0128-2021-0005).

Credit author statement

Koukina Sofia: Conceptualization, Investigation, Methodology, Writing – original draft preparation, Lobus Nikolay: Investigation, Resources, Validation, Writing – review & editing, Shatrin Aleksander: Software, Data curation, Formal analysis, Visualization

Declaration of competing interest

The authors declare that they have no known competing financial interests or personal relationships that could have appeared to influence the work reported in this paper.

Appendix A. Supplementary data

Supplementary data to this article can be found online at <https://doi.org/10.1016/j.chemosphere.2021.130951>.

References

- Barats, A., Renac, C., Orani, A.M., Durrieu, G., Saint Martin, H., Esteller, M.V., Garrido Hoyos, S.E., 2020. Tracing source and mobility of arsenic and trace elements in a hydrosystem impacted by past mining activities (Morelos state, Mexico). *Sci. Total Environ.* 712, 135565. <https://doi.org/10.1016/j.scitotenv.2019.135565>.
- Baturin, G.N., Lobus, N.V., Peresypkin, V.I., Komov, V.T., 2014. Geochemistry of channel drifts of the Kai River (Vietnam) and sediments of its mouth zone. *Oceanology* 54, 788–797. <https://doi.org/10.1134/S0001437014050026>.
- Bianchi, T.S., 2007. Biogeochemistry of Estuaries. Oxford University Press. <https://doi.org/10.1093/oso/9780195160826.001.0001>.
- Costa-Böddeker, S., Hoelzmann, P., Thuyễn, L.X., Huy, H.D., Nguyen, H.A., Richter, O., Schwalb, A., 2017. Ecological risk assessment of a coastal zone in Southern Vietnam: spatial distribution and content of heavy metals in water and surface sediments of the Thi Vai Estuary and Can Gio Mangrove Forest. *Mar. Pollut. Bull.* 114, 1141–1151. <https://doi.org/10.1016/j.marpolbul.2016.10.046>.
- Cuong, L.P., Van Tho, L., Juszakova, T., 2019. Aquatic geochemistry status in the south, central, and highland regions of Vietnam. *Environ. Sci. Pollut. Res.* 26, 21925–21947. <https://doi.org/10.1007/s11356-019-05448-9>.
- da Conceição, F.T., Fernandes, A.M., Hissler, C., Lupinacci, C.M., Menegário, A.A., Moruzzi, R.B., 2020. Multi-tracer analysis to estimate the historical evolution of pollution in riverbed sediment of subtropical watershed, the lower course of the Piracicabe River, São Paulo, Brazil. *Sci. Total Environ.* 743, 140730. <https://doi.org/10.1016/j.scitotenv.2020.140730>.
- Dyrssen, D.W., 2010. Conservative elements. *Mar. Chem. Geochemistry. A Deriv. Encycl. Ocean Sci.*
- Fernandes, L.L., Kessarkar, P.M., Rao, V.P., Suja, S., Parthiban, G., Kurian, S., 2019. Seasonal distribution of trace metals in suspended particulate and bottom sediments of four microtidal river estuaries, west coast of India. *Hydrol. Sci. J.* 64, 1519–1534. <https://doi.org/10.1080/02626667.2018.1655147>.
- Gaillardet, J., Viers, J., Dupré, B., 2014. Trace elements in river waters. *Treatise on Geochemistry*. Elsevier, pp. 195–235. <https://doi.org/10.1016/B978-0-08-095975-7.00507-6>.
- Gaonkar, C.V., Matta, V.M., 2019. Impact of mining on metal concentration in waters of the Zuarí estuary, India. *Environ. Monit. Assess.* 191, 368. <https://doi.org/10.1007/s10661-019-7506-0>.
- Giuliani, S., Bellucci, L.G., Nhon, D.H., 2019. The coast of Vietnam: present status and future challenges for sustainable development. *World Seas: an Environmental Evaluation*. Elsevier, pp. 415–435. <https://doi.org/10.1016/B978-0-08-100853-9.00027-0>.
- Grygar, T.M., Popelka, J., 2016. Revisiting geochemical methods of distinguishing natural concentrations and pollution by risk elements in fluvial sediments. *J. Geochem. Explor.* 170, 39–57. <https://doi.org/10.1016/j.gexplo.2016.08.003>.
- Guinoiseau, D., Bouchez, J., Gélibert, A., Louvat, P., Filizola, N., Benedetti, M.F., 2016. The geochemical filter of large river confluences. *Chem. Geol.* 441, 191–203. <https://doi.org/10.1016/j.chemgeo.2016.08.009>.
- Huang, Z., Liu, C., Zhao, X., Dong, J., Zheng, B., 2020. Risk assessment of heavy metals in the surface sediment at the drinking water source of the Xiangjiang River in South China. *Environ. Sci. Eur.* 32, 23. <https://doi.org/10.1186/s12302-020-00305-w>.
- Iglesias, I., Almeida, C.M.R., Teixeira, C., Mucha, A.P., Magalhães, A., Bio, A., Bastos, L., 2020. Linking contaminant distribution to hydrodynamic patterns in an urban estuary: the Douro estuary test case. *Sci. Total Environ.* 707, 135792. <https://doi.org/10.1016/j.scitotenv.2019.135792>.
- Johannesson, K.H., Palmore, C.D., Fackrell, J., Prouty, N.G., Swarzenski, P.W., Chevis, D.A., Telfeyan, K., White, C.D., Burdige, D.J., 2017. Rare earth element behavior during groundwater-seawater mixing along the Kona Coast of Hawaii. *Geochim. Cosmochim. Acta* 198, 229–258. <https://doi.org/10.1016/j.gca.2016.11.009>.
- Jones, D.L., 2017. Fathom Toolbox for matlab | USF college of marine science (accessed 4.26.21). <https://www.usf.edu/marine-science/research/matlab-resources/fathom-toolbox-for-matlab.aspx>.
- Kaotekwar, A.B., Ahmad, S.M., Satyanarayanan, M., Krishna, A.K., 2019. Geochemical investigations in bulk and clay size fractions from lower Krishna river sediments, southern India: implications of elemental fractionation during weathering, transportation and deposition. *Geosci. J.* 23, 951–960. <https://doi.org/10.1007/s12303-019-0002-2>.
- Karandashev, V.K., Turanov, A.N., Orlova, T.A., Lezhnev, A.E., Nosenko, S.V., Zolotareva, N.I., Moskvitina, I.R., 2008. Use of the inductively coupled plasma mass spectrometry for element analysis of environmental objects. *Inorg. Mater.* 44, 1491–1500. <https://doi.org/10.1134/S0020168508140045>.
- Karpov, Y.A., Orlova, V.A., 2008. Modern methods of autoclave sample preparation in chemical analysis of substances and materials. *Inorg. Mater.* 44, 1501–1508. <https://doi.org/10.1134/S0020168508140057>.
- Khoi, N.N., 2014. Mineral Resources potential of Vietnam and current state of mining activity. *Appl. Environ. Res.* 36, 37–46. <https://doi.org/10.35762/AER.2014.36.1.6>.
- Koiter, A.J., Owens, P.N., Petticrew, E.L., Lobb, D.A., 2013. The behavioural characteristics of sediment properties and their implications for sediment fingerprinting as an approach for identifying sediment sources in river basins. *Earth Sci. Rev.* 125, 24–42. <https://doi.org/10.1016/j.earscirev.2013.05.009>.
- Koukina, S., Lobus, N., 2019. Major and trace element distribution in suspended particulate matter and sediments of the tropical river estuary (south Vietnam). In: Chaminé, H.I. (Ed.), *Advances in Sustainable and Environmental Hydrology, Hydrogeology, Hydrochemistry and Water Resources*. Springer Nature, Switzerland AG, pp. 65–67. https://doi.org/10.1007/978-3-030-01572-5_16.
- Koukina, S., Lobus, N., 2018. Trace elements in suspended particulate matter and sediments of the Cai River: Nha Trang bay estuarine system (south China sea). *Trace Elements - Human Health and Environment*. InTech. <https://doi.org/10.5772/intechopen.76471>.
- Koukina, S.E., Lobus, N.V., Peresypkin, V.I., Dara, O.M., Smurov, A.V., 2017. Abundance, distribution and bioavailability of major and trace elements in surface sediments from the Cai River estuary and Nha Trang bay (south China sea, Vietnam). *Estuar. Coast Shelf Sci.* 198, 450–460. <https://doi.org/10.1016/j.ecss.2016.03.005>.

- Koukina, S.E., Lobus, N.V., 2020. Relationship between enrichment, toxicity, and chemical bioavailability of heavy metals in sediments of the Cai River estuary. *Environ. Monit. Assess.* 192, 305. <https://doi.org/10.1007/s10661-020-08282-6>.
- Lasareva, E.V., Parfenova, A.M., Romanovich, E.A., Lobus, N.V., Drozdova, A.N., 2019. Organic matter and mineral interactions modulate flocculation across arctic river mixing zones. *J. Geophys. Res. Biogeosciences* 124, 1651–1664. <https://doi.org/10.1029/2019JG005026>.
- Legendre, P., 2019. Numerical ecology. *Encyclopedia of Ecology*. Elsevier, pp. 487–493. <https://doi.org/10.1016/B978-0-12-409548-9.10595-0>.
- Li, L., Liu, H., Li, H., 2018. Distribution and migration of antimony and other trace elements in a Karstic river system, Southwest China. *Environ. Sci. Pollut. Res.* 25, 28061–28074. <https://doi.org/10.1007/s11356-018-2837-x>.
- Lima, G.F.C., Bento, C.C., Horn, A.H., Marques, E.D., Filho, H.B., 2021. Geochemical signature and environmental background of bottom sediments in a tropical aquatic system: the Três Marias Reservoir, Brazil. *Environ. Monit. Assess.* 193 <https://doi.org/10.1007/s10661-021-08876-8>.
- Lobus, N.V., Komov, V.T., 2016. Mercury in the muscle tissue of fish in the central and south Vietnam. *Inl. Water Biol.* 9, 319–328. <https://doi.org/10.1134/S1995082916030159>.
- Lobus, N.V., Komov, V.T., Thanh, N.T.H., 2011. Mercury concentration in ecosystem components in water bodies and streams in Khanh Hoa province (Central Vietnam). *Water Resour.* 38, 799–805. <https://doi.org/10.1134/S0097807811060091>.
- Lobus, N.V., Peresypkin, V.I., Shulga, N.A., Drozdova, A.N., Gusev, E.S., 2015. Dissolved, particulate, and sedimentary organic matter in the Cai River basin (Nha Trang bay of the south China sea). *Oceanology* 55, 339–346. <https://doi.org/10.1134/S0001437015030121>.
- Loring, D.H., Rantala, R.T.T., 1992. Manual for the geochemical analyses of marine sediments and suspended particulate matter. *Earth Sci. Rev.* 32, 235–283. [https://doi.org/10.1016/0012-8252\(92\)90001-A](https://doi.org/10.1016/0012-8252(92)90001-A).
- Lounas, R., Kasmi, H., Chernai, S., Amarni, N., Hamdi, B., 2020. Assessing the contamination and ecological risk of sediments around the mariculture area in northern Algeria using a multivariate approach. *J. Appl. Aquacult.* <https://doi.org/10.1080/10454438.2020.1823297>.
- Mali, M., Dell'Anna, M.M., Notarnicola, M., Damiani, L., Mastrolilli, P., 2017. Combining chemometric tools for assessing hazard sources and factors acting simultaneously in contaminated areas: Case study: "Mar Piccolo" Taranto (South Italy). *Chemosphere* 184, 784–794. <https://doi.org/10.1016/j.chemosphere.2017.06.028>.
- Mali, M., Ungaro, N., Cardellinichio, A., Dell'Anna, M.M., Romanazzi, G., Mastrolilli, P., Damiani, L., 2019. Long-term monitoring programs to assess environmental pressures on coastal area: weighted indexes and statistical elaboration as handy tools for decision-makers. *Ecol. Indicat.* 101, 838–850. <https://doi.org/10.1016/j.ecolind.2019.01.085>.
- Moore, D.M., Reynolds, R.C., 1989. *X-ray Diffraction and the Identification and Analysis of Clay minerals*, X-Ray Diffraction and the Identification and Analysis of Clay Minerals. Oxford University Press (OUP), Oxford.
- Naumov, A.V., 2007. World market of bismuth: a review. *Russ. J. Non-Ferrous Metals*. <https://doi.org/10.3103/S1067821207010038>.
- Nozaki, Y., 2010. Element distribution: overview. *Mar. Chem. Geochemistry. A Deriv. Encycl. Ocean Sci.*
- Ojebuoboh, F.K., 1992. Bismuth - production, properties, and applications. *J. Occup. Med.* 44, 46–49. <https://doi.org/10.1007/BF03222821>.
- Orlova, V.A., 2003. Analytical Autoclaves: Autoclave Preparation of Samples in Chemical Analysis. Central Scientific Research Institute of Agrochemical Service of Agriculture Moscow, Moscow.
- Peresypkin, V.I., Smurov, A.V., Shulga, N.A., Safonova, E.S., Smurova, T.G., Bang, C.V., 2011. Composition of the organic matter of the water, suspended matter, and bottom sediments in Nha Trang Bay in Vietnam in the South China Sea. *Oceanology* 51, 959–968. <https://doi.org/10.1134/S0001437011060130>.
- Prabakaran, K., Nagarajan, R., Eswaramoorthy, S., Anandkumar, A., Franco, F.M., 2019. Environmental significance and geochemical speciation of trace elements in Lower Baram River sediments. *Chemosphere*. <https://doi.org/10.1016/j.chemosphere.2018.11.158>.
- Romano, S., Mugnai, C., Cu, N.H., Giuliani, S., Belluccini, L.G., Turetta, C., Capodaglio, G., Nhon, D.H., Albertazzi, S., Frignani, M., 2013. Extreme events and environmental changes: tracing sedimentary processes in Central Vietnam coastal lagoons. *Chem. Ecol.* <https://doi.org/10.1080/02757540.2012.711321>.
- Rousseau, T.C.C., Roddaz, M., Moquet, J.-S., Handt Delgado, H., Calves, G., Bayon, G., 2019. Controls on the geochemistry of suspended sediments from large tropical South American rivers (Amazon, Orinoco and Maroni). *Chem. Geol.* 522, 38–54. <https://doi.org/10.1016/j.chemgeo.2019.05.027>.
- Sang, P.N., Liu, Z., Stattegger, K., 2019. Weathering and erosion in central Vietnam over the holocene and younger dryas: clay mineralogy and elemental geochemistry from the Vietnam shelf, western south China sea. *J. Asian Earth Sci.* 179, 1–10. <https://doi.org/10.1016/j.jseas.2019.04.008>.
- Savenko, V.S., 2006. Chemical composition of World River's suspended matter. *Geos. Sholkovitz, E., Szymczak, R., 2000. The estuarine chemistry of rare earth elements: comparison of the Amazon, Fly, Sepik and the Gulf of Papua systems. *Earth Planet Sci. Lett.* 179, 299–309. [https://doi.org/10.1016/S0012-821X\(00\)00112-6](https://doi.org/10.1016/S0012-821X(00)00112-6).*
- Strady, E., Dang, V.B.H., Némery, J., Guédron, S., Dinh, Q.T., Denis, H., Nguyen, P.D., 2017a. Baseline seasonal investigation of nutrients and trace metals in surface waters and sediments along the Saigon River basin impacted by the megacity of Ho Chi Minh (Vietnam). *Environ. Sci. Pollut. Res.* 24, 3226–3243. <https://doi.org/10.1007/s11356-016-7660-7>.
- Strady, E., Dinh, Q.T., Némery, J., Nguyen, T.N., Guédron, S., Nguyen, N.S., Denis, H., Nguyen, P.D., 2017b. Spatial variation and risk assessment of trace metals in water and sediment of the Mekong Delta. *Chemosphere* 179, 367–378. <https://doi.org/10.1016/j.chemosphere.2017.03.105>.
- Stutter, M.I., Langan, S.J., Lumsdon, D.G., Clark, L.M., 2009. Multi-element signatures of stream sediments and sources under moderate to low flow conditions. *Appl. Geochemistry*. <https://doi.org/10.1016/j.apgeochem.2009.01.005>.
- Thanh-Nho, N., Marchand, C., Strady, E., Vinh, T.-V., Nhu-Trang, T.-T., 2019. Metals geochemistry and ecological risk assessment in a tropical mangrove (Can Gio, Vietnam). *Chemosphere* 219, 365–382. <https://doi.org/10.1016/j.chemosphere.2018.11.163>.
- Thanh-Nho, N., Strady, E., Nhu-Trang, T., David, F., Marchand, C., 2018. Trace metals partitioning between particulate and dissolved phases along a tropical mangrove estuary (Can Gio, Vietnam). *Chemosphere* 196, 311–322. <https://doi.org/10.1016/j.chemosphere.2017.12.189>.
- Thuong, N.T., Yoneda, M., Shimada, Y., Matsui, Y., 2015. Assessment of trace metal contamination and exchange between water and sediment systems in the to Lich River in inner Hanoi, Vietnam. *Environ. Earth Sci.* 73, 3925–3936. <https://doi.org/10.1007/s12665-014-3678-7>.
- Tomczak, W., Boyer, P., Krimissa, M., Radakowitch, O., 2019. Kd distributions in freshwater systems as a function of material type, mass-volume ratio, dissolved organic carbon and pH. *Appl. Geochemistry* 105, 68–77. <https://doi.org/10.1016/j.apgeochem.2019.04.003>.
- Tomilina, I.I., Grebenyuk, L.P., Lobus, N.V., Komov, V.T., 2016. Biological effects of contaminated bottom sediments of water bodies in Central and South Vietnam on aquatic organisms. *Inl. Water Biol.* 9, 413–422. <https://doi.org/10.1134/S1995082916030196>.
- Tran, T.A.M., Leermakers, M., Hoang, T.L., Nguyen, V.H., Elskens, M., 2018. Metals and arsenic in sediment and fish from Cau Hai lagoon in Vietnam: ecological and human health risks. *Chemosphere* 210, 175–182. <https://doi.org/10.1016/j.chemosphere.2018.07.002>.
- Turekian, K.K., Wedepohl, K.H., 1961. Distribution of the elements in some major units of the earth's crust. *Bull. Geol. Soc. Am.* 72, 175–192. [https://doi.org/10.1130/0016-7660\(1961\)72\[175:DOTEIS\]2.0.CO;2](https://doi.org/10.1130/0016-7660(1961)72[175:DOTEIS]2.0.CO;2).
- Turner, A., 1996. Trace-metal partitioning in estuaries: importance of salinity and particle concentration. *Mar. Chem.* 54, 27–39. [https://doi.org/10.1016/0304-4203\(96\)00025-4](https://doi.org/10.1016/0304-4203(96)00025-4).
- Turner, A., Millward, G.E., Bale, A.J., Morris, A.W., 1993. Application of the KD concept to the study of trace metal removal and desorption during estuarine mixing. *Estuar. Coast Shelf Sci.* 36, 1–13. <https://doi.org/10.1006/ecss.1993.1001>.
- US EPA, 2006. National recommended water quality criteria [WWW document] (accessed 11.16.20). <https://www.epa.gov/wqc/national-recommended-water-quality-criteria-aquatic-life-criteria-table>.
- Varol, M., 2011. Assessment of heavy metal contamination in sediments of the Tigris River (Turkey) using pollution indices and multivariate statistical techniques. *J. Hazard Mater.* 195, 355–364. <https://doi.org/10.1016/j.jhazmat.2011.08.051>.
- Viers, J., Dupré, B., Gaillardet, J., 2009. Chemical composition of suspended sediments in World Rivers: new insights from a new database. *Sci. Total Environ.* 407, 853–868. <https://doi.org/10.1016/j.scitotenv.2008.09.053>.
- World Health Organization, 2006. Guidelines for the safe use of wastewater, excreta and greywater - volume 2 [WWW Document]. WHO, URL, accessed 11.16.20. http://www.who.int/water_sanitation_health/publications/gsuweg2/en/.
- Xie, Y., Hou, Z., Xu, J., Yuan, Z., Bai, G., Li, X., 2006. Discovery of Cu-Zn, Cu-Sn intermetallic minerals and its significance for genesis of the mianning-dechang REE metallogenic belt, sichuan province, China. *Sci. China, ser. Dokl. Earth Sci.* 49, 597–603. <https://doi.org/10.1007/s11430-006-0597-9>.
- Yao, Q., Wang, X., Jian, H., Chen, H., Yu, Z., 2016. Behavior of suspended particles in the Changjiang Estuary: size distribution and trace metal contamination. *Mar. Pollut. Bull.* 103, 159–167. <https://doi.org/10.1016/j.marpolbul.2015.12.026>.